Alexandria Engineering Journal (2016) 55, 653–662

HOSTED BY

ELSEVIER

Alexandria University

Alexandria Engineering Journal

www.elsevier.com/locate/aej
www.sciencedirect.com

ORIGINAL ARTICLE

Three dimensional peristaltic flow of hyperbolic tangent fluid in non-uniform channel having flexible walls

M. Ali Abbas [a], **Y.Q. Bai** [a], **M.M. Bhatti** [b,*], **M.M. Rashidi** [c,d]

[a] *Department of Mathematics, Shanghai University, Shanghai 200444, China*
[b] *Shanghai Institute of Applied Mathematics and Mechanics, Shanghai University, Yanchang Road, Shanghai 200072, China*
[c] *Shanghai Key Lab of Vehicle Aerodynamics and Vehicle Thermal Management Systems, Tongji University, Shanghai 201804, China*
[d] *ENN-Tongji Clean Energy Institute of Advanced Studies, Shanghai 200072, China*

Received 10 May 2015; revised 30 September 2015; accepted 28 October 2015
Available online 23 November 2015

KEYWORDS

Peristaltic flow;
Hyperbolic tangent fluid;
Non-uniform channel;
Analytic solution

Abstract In this present analysis, three dimensional peristaltic flow of hyperbolic tangent fluid in a non-uniform channel has been investigated. We have considered that the pressure is uniform over the whole cross section and the interial effects have been neglected. For this purpose we consider laminar flow under the assumptions of long wavelength ($\lambda \to \infty$) and creeping flow ($Re \to 0$) approximations. The attained highly nonlinear equations are solved with the help of Homotopy perturbation method. The influence of various physical parameters of interest is demonstrated graphically for wall tension, mass characterization, damping nature of the wall, wall rigidity, wall elastance, aspect ratio and the Weissenberg number. In this present investigation we found that the magnitude of the velocity is maximum in the center of the channel whereas it is minimum near the walls. Stream lines are also drawn to discuss the trapping mechanism for all the physical parameters. Comparison has also been presented between Newtonian and non-Newtonian fluid.

1. Introduction

In recent decades, peristaltic flow has gained a remarkable interest due to its lot of application in distinct field of sciences. In particular, it is mechanism of transporting the fluid in various biological systems. Several applications of peristalsis are transport of urine from kidney to bladder through ureter, swallowing food through esophagus, transport of spermatozoa induct efferent of male reproductive system tract, movement of ovum in female fallopian tube, swallowing of food through esophagus, transport of lymph in lymphatic vessels such as arterioles, capillaries, venules. An innumerable application of peristaltic pumping has been found in corrosive fluid or sensitive fluids, sanitary fluids, transport of slurries and noxious fluids in nuclear industry. After an impressive work of Lytham [1], many authors investigated analytically and experimentally the mechanism of peristalsis [2–20]. Shit and Roy [21] investigated peristaltic motion of couple stress fluid under the influ-

* Corresponding author.
E-mail addresses: mubashirme@yahoo.com, muhammad09@shu.edu.cn (M.M. Bhatti).
Peer review under responsibility of Faculty of Engineering, Alexandria University.

http://dx.doi.org/10.1016/j.aej.2015.10.012
1110-0168 © 2015 Faculty of Engineering, Alexandria University. Production and hosting by Elsevier B.V.

Nomenclature

u, w	velocity components in x and y directions in wave frame	ψ	stream function
x, y, z	Cartesian coordinate system	a	height of the channel
ρ	constant density	b	amplitude of the wave
Γ	time constant	Π	second invariant tensor
n	power law index	ϕ	amplitude ratio
Re	Reynolds number	d	width of the channel
β	aspect ratio	p	pressure
λ	wavelength	η_∞	infinite shear rate viscosity
c	velocity of propagation	η_0	zero shear rate viscosity
δ	ratio of height to wavelength	$\mathbf{S}$	stress tensor
		We	Weissenberg number

ence of hydromagnetic effects with the numerical scheme. His results depict that trapping fluid can be removed and the axial velocity can be decreased with the help of magnetic field. Mittra et al. [22] discussed the influence of wall properties and Poiseuille flow in peristalsis. He analyzed that the mean flow reversal existing at the boundaries and also at the center of the channel. He observed that due to elasticity in the walls of channel, there is flow reversal at the center of the channel.

Later, Mittra et al. [23] also studied the interaction of peristaltic motion with Poiseuille flow. He found that flow reversal is mainly dependent on the Poiseuille flow and the flow reversal is versatile from the center to the boundaries of the channel. Rashidi et al. [24] analyzed analytically the effects of heat transfer through a porous annulus with pulsating pressure gradient. Das et al. [25] numerically analyzed the variable fluid properties over permeable surface under the impact of thermophoretic Magnetohydrodynamics (MHD) slip flow. He assumed that magnetic field is a function of time and also he supposed that thermal conductivity and viscosity of the liquid vary as a linear and inverse function of temperature. He found that the thermal boundary layer thickness shows opposite behavior for viscosity parameter and surface convection parameter. Recently, Ellahi et al. [26] examined the mathematical analysis of peristaltic transport of an eyring powell fluid through a porous rectangular duct. Ellahi et al. [27] investigated the peristaltic flow in a non-uniform rectangular duct under the effects of heat and mass transfer. Recently Akram et al. [28] studied the Influence of lateral walls on peristaltic flow of a couple stress fluids in a non-uniform rectangular duct. Ellahi et al. [29] examined the peristaltic flow of Jeffrey in a rectangular duct under the effects of magnetic field through porous walls. He analyzed that due to the effects of magnetic field and porosity the velocity of the fluid decreases. Reddy [30] evaluated the influence of lateral walls on peristaltic flow in a rectangular duct. Riaz et al. [31] studied the peristaltic motion of three dimensional non-Newtonian Carreau fluid having compliant walls. He found that with the increment of parameter wall tension and mass characterization, the velocity of the fluid decreases whereas its behavior is opposite for the remaining parameters. He also observed that the fluid velocity is maximum at the middle of the channel. Shapiro et al. [32] studied the peristaltic pumping with long wavelengths at low Reynolds number. Rashidi et al. [33] described the pulsatile flow in a porous medium with the help of homotopy analysis method. Mekheimer [34] considered the peristaltic flow of blood under effect of a magnetic field in a non-uniform channels. Elnaby and Haroun [35] have investigated a new model for studying the effect of wall properties on peristaltic transport of a viscous fluid. Effects of hall currents on peristaltic transport with compliant walls were explored by Gad [36]. Mekheimer et al. [37] analyzed the endoscopic mechanism on peristaltic flow through a porous medium in an annulus. According to best of authors knowledge three dimensional peristaltic flow of hyperbolic tangent fluid in non-uniform duct of rectangular cross section with compliant walls has not yet been observed.

With above analysis in mind, we are interested in analytical approximation of peristaltic flow in non-uniform channel of rectangular cross section with compliant walls. We considered the flow under the assumptions of long wavelength and low Reynolds number approximation. The reduced highly nonlinear partial differential equations are solved with help of homotopy perturbation technique [38–42]. Homotopy perturbation method is an analytic method that is used to solve many peristaltic flow problems. Closed form solutions up to first order are presented. The impact of various pertinent parameters is plotted and discussed. The most interesting mechanism of peristalsis is trapping which is also taken into account by drawing stream of all the physical parameters.

2. Mathematical formulation

We consider the in-compressible hyperbolic tangent fluid in non-uniform duct of rectangular cross section. We have elected Cartesian coordinate system i.e. $x-axis$ is taken along the axial direction, $y-axis$ is taken along the lateral direction and $z-axis$ is taken along the vertical direction of the non-uniform channel as shown in Fig. 1.

The peristaltic waves on the walls can be written as [27]

$$\mathbf{H}(x,t) = \pm a + \mathbf{K}x \pm b\cos\frac{2\pi}{\lambda}(x-ct), \tag{1}$$

The walls parallel to xz plane are not interrupted and don't participate to any peristaltic wave motion. Let $(u, 0, w)$ be the velocity for the flow in a channel. The governing equations for the Hyperbolic Tangent fluid are defined as

$$\frac{\partial u}{\partial x} + \frac{\partial w}{\partial z} = 0, \tag{2}$$

$$\rho\left(\frac{\partial u}{\partial t} + u\frac{\partial u}{\partial x} + w\frac{\partial u}{\partial z}\right) = -\frac{\partial p}{\partial x} + \frac{\partial}{\partial x}\mathrm{S}_{xx} + \frac{\partial}{\partial y}\mathrm{S}_{xy} + \frac{\partial}{\partial z}\mathrm{S}_{xz}, \tag{3}$$

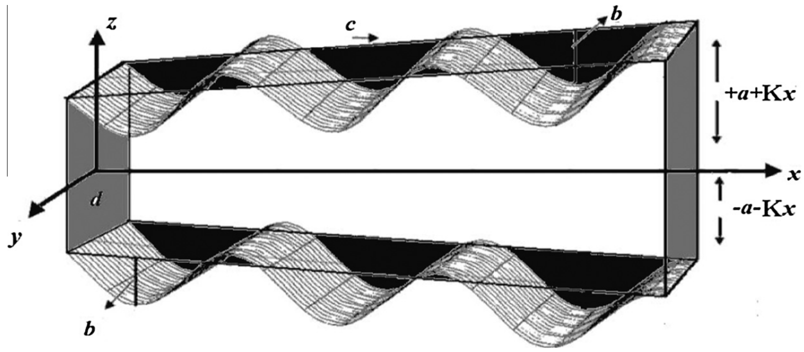

Figure 1 Geometry of the problem.

$$0=-\frac{\partial p}{\partial y}+\frac{\partial}{\partial x}\mathrm{S}_{yx}+\frac{\partial}{\partial y}\mathrm{S}_{yy}+\frac{\partial}{\partial z}\mathrm{S}_{yz}, \tag{4}$$

$$\rho\left(\frac{\partial w}{\partial t}+u\frac{\partial w}{\partial x}+w\frac{\partial w}{\partial z}\right)=-\frac{\partial p}{\partial z}+\frac{\partial}{\partial x}\mathrm{S}_{zx}+\frac{\partial}{\partial y}\mathrm{S}_{zy}+\frac{\partial}{\partial z}\mathrm{S}_{zz}, \tag{5}$$

The stress tensor for hyperbolic Tangent fluid is defined as [43]

$$\mathbf{S}=-\left[\left(\eta_\infty+(\eta_0+\eta_\infty)\tanh\left(\Gamma\bar{\dot{\gamma}}\right)^n\right)\dot{\gamma}\right], \tag{6}$$

In the above equation

$$\bar{\dot{\gamma}}=\sqrt{\frac{1}{2}\sum_i\sum_j\dot{\gamma}_{ij}\gamma_{ji}}=\sqrt{\frac{1}{2}\Pi}, \tag{7}$$

$$\Pi=\mathrm{trac}\left(grad\mathbf{V}+(grad\mathbf{V})^T\right)^2, \tag{8}$$

We consider the case for which $\eta_\infty=0$ and $\Gamma\dot{\gamma}<1$ in Eq. (6). Therefore the component for the stress tensor can be described as

$$\mathbf{S}=-\eta_0\left[\left(\Gamma\dot{\gamma}\right)^n\right]\dot{\gamma}=-\eta_0\left[1+n\left(\Gamma\dot{\gamma}-1\right)\right]\dot{\gamma}. \tag{9}$$

Introducing the following non-dimensional quantities

$$\begin{gathered}\tilde{x}=\frac{x}{\lambda},\ \tilde{y}=\frac{y}{d},\ \tilde{z}=\frac{z}{a},\ \tilde{u}=\frac{u}{c},\ \tilde{w}=\frac{w}{c\delta},\ \tilde{t}=\frac{ct}{\lambda},\ k=\frac{\lambda\mathbf{K}}{a},\\ \mathbb{H}=\frac{\mathbf{H}}{a},\ \tilde{p}=\frac{ap}{\mu c\lambda},\\ \mathrm{Re}=\frac{\rho ac}{\mu},\ \delta=\frac{a}{\lambda},\ \phi=\frac{b}{a},\ \mathrm{S}_{\tilde{x}\tilde{x}}=\frac{a}{\mu c}\mathrm{S}_{xx},\ \mathrm{S}_{\tilde{x}\tilde{y}}=\frac{d}{\mu c}\mathrm{S}_{xy},\\ \mathrm{S}_{\tilde{x}\tilde{z}}=\frac{a}{\mu c}\mathrm{S}_{xz},\\ \mathrm{S}_{\tilde{y}\tilde{z}}=\frac{d}{\mu v}\mathrm{S}_{yz},\ \mathrm{S}_{\tilde{z}\tilde{z}}=\frac{\lambda}{\mu c}\mathrm{S}_{zz},\ \mathrm{S}_{\tilde{y}\tilde{y}}=\frac{\lambda}{\mu c}\mathrm{S}_{yy},\ \beta=\frac{a}{d},\ We=\frac{\Gamma c}{a},\\ \tilde{\dot{\gamma}}=\frac{\dot{\gamma}a}{c}.\end{gathered} \tag{10}$$

Using the above non-dimensional quantities in Eqs. (2)–(10), the resulting equations after dropping the tilde can be written as

$$\frac{\partial u}{\partial x}+\frac{\partial w}{\partial z}=0, \tag{11}$$

$$\mathrm{Re}\delta\left(\frac{\partial u}{\partial t}+u\frac{\partial u}{\partial x}+w\frac{\partial u}{\partial z}\right)=-\frac{\partial p}{\partial x}+\delta\frac{\partial}{\partial x}\mathrm{S}_{xx}+\beta^2\frac{\partial}{\partial y}\mathrm{S}_{xy}+\frac{\partial}{\partial z}\mathrm{S}_{xz}, \tag{12}$$

$$0=-\frac{\partial p}{\partial y}+\delta^2\frac{\partial}{\partial x}\mathrm{S}_{yx}+\delta^2\frac{\partial}{\partial y}\mathrm{S}_{yy}+\delta\frac{\partial}{\partial z}\mathrm{S}_{yz}, \tag{13}$$

$$\mathrm{Re}\delta^2\left(\frac{\partial w}{\partial t}+u\frac{\partial w}{\partial x}+w\frac{\partial w}{\partial z}\right)=-\frac{\partial p}{\partial z}+\delta^2\frac{\partial}{\partial x}\mathrm{S}_{zx}+\delta\beta^2\frac{\partial}{\partial y}\mathrm{S}_{zy}+\delta^2\frac{\partial}{\partial z}\mathrm{S}_{zz}, \tag{14}$$

We consider the assumption of long wavelength $\lambda\to\infty$ and low Reynolds number $Re\to 0$ approximation. Then from Eqs. (12)–(14) reduces to the following form

$$\frac{\partial p}{\partial x}=\beta^2(1-n)\frac{\partial^2 u}{\partial y^2}+n\beta^4 We\frac{\partial}{\partial y}\left(\frac{\partial u}{\partial y}\right)^3+(1-n)\frac{\partial^2 u}{\partial z^2}+nWe\frac{\partial}{\partial z}\left(\frac{\partial u}{\partial z}\right)^3. \tag{15}$$

The corresponding boundary conditions are

$$\begin{aligned}u(y,z)&=-1, \qquad (y=\pm 1),\\ u(y,z)&=-1, \qquad (z=\pm\mathbb{H}),\end{aligned} \tag{16}$$

where $0\leqslant\phi\leqslant 1$, $\mathbb{H}=1+kx+\zeta(x,t)$ and $\zeta(x,t)=\phi\cos 2\pi(x-t)$. The expression for the compliant wall can be defined as

$$\mathbb{L}(\zeta)=p-p_o, \tag{17}$$

where p_0 is pressure on outside surface of the wall due to tension in muscle, which is assumed to be zero here. The $\mathbb{L}$ operator is used to described the of stretched membrane with viscosity damping force such as

$$\mathbb{L}=\mathbb{M}\frac{\partial^2}{\partial t^2}+\mathbb{D}\frac{\partial}{\partial t}+\mathbb{B}\frac{\partial^4}{\partial x^4}-\mathbb{T}\frac{\partial^2}{\partial x^2}+\mathbb{K}, \tag{18}$$

In the above equation, $\mathbb{M}$ is mass per unit area, $\mathbb{D}$ is coefficient of the viscosity damping membrane, $\mathbb{B}$ is flexural rigidity of the plate, $\mathbb{T}$ is elastic tension in the membrane and $\mathbb{K}$ is spring stiffness. Using Eqs. (17) and (18) we get

$$\frac{\partial p}{\partial x}=\mathbb{E}_1\frac{\partial^3\zeta}{\partial t^2\partial x}+\mathbb{E}_2\frac{\partial^2\zeta}{\partial t\partial x}+\mathbb{E}_3\frac{\partial^5\zeta}{\partial x^5}-\mathbb{E}_5\frac{\partial^3\zeta}{\partial x^3}+\mathbb{E}_5\frac{\partial\zeta}{\partial x}, \tag{19}$$

Rewriting Eq. (15) with the help of Eq. (19) we get

$$\beta^2(1-n)\frac{\partial^2 u}{\partial y^2}+n\beta^4 We\frac{\partial}{\partial y}\left(\frac{\partial u}{\partial y}\right)^3+(1-n)\frac{\partial^2 u}{\partial z^2}+nWe\frac{\partial}{\partial z}\left(\frac{\partial u}{\partial z}\right)^3=\mathbb{E}_1\frac{\partial^3\zeta}{\partial t^2\partial x}+\mathbb{E}_2\frac{\partial^2\zeta}{\partial t\partial x}+\mathbb{E}_3\frac{\partial^5\zeta}{\partial x^5}-\mathbb{E}_5\frac{\partial^3\zeta}{\partial x^3}+\mathbb{E}_5\frac{\partial\zeta}{\partial x}, \tag{20}$$

in the above equation $\mathbb{E}_1 = \mathbb{M}a^3c/\lambda^3\mu$, $\mathbb{E}_2 = \mathbb{D}a^3/\lambda^2\mu$, $\mathbb{E}_3 = \mathbb{B}a^3/c\lambda^5\mu$, $\mathbb{E}_4 = \mathbb{T}a^3/c\lambda^3\mu$ and $\mathbb{E}_5 = \mathbb{K}a^3/c\lambda\mu$ are the non-dimensional elasticity quantities.

3. Solution of the problem

The homotopy perturbation method for the above nonlinear partial differential equation can be defined as

$$\hbar(v,\mathbb{k}) = (1-\mathbb{k})(\mathfrak{L}(v) - \mathfrak{L}(\tilde{v}_0)) + \mathbb{k}\left(\mathfrak{L}(v) + n\beta^4 We\frac{\partial}{\partial y}\left(\frac{\partial u}{\partial y}\right)^3 + nWe\frac{\partial}{\partial z}\left(\frac{\partial u}{\partial z}\right)^3 - \mathbb{C}\right). \tag{21}$$

We have selected the following linear operator as

$$\mathfrak{L} = \beta^2(1-n)\frac{\partial^2}{\partial y^2} + (1-n)\frac{\partial^2}{\partial z^2}, \tag{22}$$

and the initial guess is defined as

$$\tilde{v}_0 = -1 + \frac{1-y^2}{\beta^2 - n\beta^2} + \frac{z^2 - \mathbb{H}^2}{1-n}, \tag{23}$$

In the above equation $n \neq 1$. Now, introducing the following expansion

$$w(y,z) = w_0 + \mathbb{k}w_1 + \mathbb{k}^2 w_2 + \cdots \tag{24}$$

Using Eqs. (21) and (24) and comparing the like powers of $\mathbb{k}$, we get a system of equations. According to the methodology of perturbation (HPM), we found the solution as $\mathbb{k} \to 1$, we get

$$u(y,z) = w(y,z)|_{\mathbb{k}\to 1} = w_0 + \mathbb{k}w_1 + \mathbb{k}^2 w_2 + \cdots \tag{25}$$

The solution for the velocity up to first order can be written as

$$\begin{aligned} u(y,z) = {} & -1 + \frac{1-y^2}{\beta^2 - n\beta^2} + \frac{z^2 - \mathbb{H}^2}{1-n} + \sum\nolimits_{m=0}^{\infty} 1/(2(n-1)^3\lambda_m^{5/2}\beta^2)2(\mathbb{H}\sqrt{\lambda_m}((n-1)^3\mathbb{C} \\ & \times \beta^2\lambda_m + 24We(-ny^2\lambda_m + \beta^2(-6 + \mathbb{H}^2\lambda_m)))) \cos\sqrt{\lambda_m}\mathbb{H} + (-(n-1)^3 \\ & \times \mathbb{C}\beta^2\lambda_m + 24We(ny^2\lambda_m + \beta^2(6 - 3\mathbb{H}^2\lambda_m)) \sin\sqrt{\lambda_m}\mathbb{H}^2/\cosh\sqrt{\lambda_m}/\beta\mathbb{H} \\ & + \sin 2\mathbb{H}\sqrt{\lambda_m}/2\sqrt{\lambda_m})(\cosh\sqrt{\lambda_m}(y/\beta)\cos\sqrt{\lambda_m}z) + (1/(2(n-1)^3\beta^2)) \\ & \times (24\mathbb{H}^2 nWey^2 - 24nWey^2z^2 + \mathbb{H}^2\mathbb{C}\beta - 3\mathbb{H}^2 n\mathbb{C}\beta^2 + 3\mathbb{H}^2n^2\mathbb{C}\beta^2 - \beta^2\mathbb{C} \\ & \times z^2 - \mathbb{H}^2n^3\mathbb{C}\beta^2 + 3n\mathbb{C}z^2\beta^2 - 3n^2\mathbb{C}z^{22} + n^3\mathbb{C}z^{22} + 12Wez^4\beta^2), \end{aligned} \tag{26}$$

where

$$\mathbb{C} = 2\pi\phi\cos 2\pi(x-t)\big((\mathbb{E}_4 - \mathbb{E}_1 + 4\pi^2\mathbb{E}_3)4\pi^2 + \mathbb{E}_5\big) + \mathbb{E}_2 4\pi^2\phi\sin 2\pi(x-t), \tag{27}$$

4. Results and discussion

4.1. Effects of different parameters on velocity profile

In this section the graphical analysis of various pertinent parameters of interest is plotted and trapping mechanism has also taken into account by drawing stream lines. For this purpose Figs. 2–13 are prepared. Figs. 2–5 describes the behavior of wall tension $\mathbb{E}_1$, mass characterization parameter $\mathbb{E}_2$, damping nature $\mathbb{E}_3$, wall rigidity $\mathbb{E}_4$, wall elastance $\mathbb{E}_5$, aspect ratio β, fluid parameter n and We on velocity and Figs. 6–13 are drawn for stream lines for the similar parameters. The stream function satisfying equation of continuity is stated as

$$u = \frac{\partial\psi}{\partial z}, \quad w = -\frac{\partial\psi}{\partial x}.$$

Fig. 2a shows that when wall tension $\mathbb{E}_1$ increases the velocity of the fluid decreases near the walls of the duct whereas it increases in the center of the duct. Fig. 2b is plotted for different values of mass characterization parameter $\mathbb{E}_2$. From this figure we analyze that when $\mathbb{E}_2$ increases the velocity of the fluid increases from the middle of the duct but its behavior is completely opposite near the walls. Fig. 3a describes that when damping nature $\mathbb{E}_3$ increases the velocity of the fluid increases in the narrower part of the duct but in the wider part of the duct its mode is different. It depicts from Fig. 3b that with the increment of wall rigidity $\mathbb{E}_4$, the velocity field increases. It can easily observed from Fig. 4a that when wall elastance $\mathbb{E}_5$ increases the velocity of the fluid increases slowly in the mean of the duct and near the walls its attitude is opposite and it decreases gradually. It can be examined from Fig. 4b that when n increases the velocity field decreases. Fig. 5a shows the impact of We on velocity. From this figure we analyze that with the rise of We the velocity field decreases near the corners of the duct but its reaction in the middle of the duct is opposite. Fig. 5b describes that when the aspect ratio β increases the velocity field decreases in the wider part of the duct whereas in the center of the duct it increases.

4.2. Trapping mechanism

The second most interesting demonstration is trapping mechanism. It depicts from Fig. 6 that when wall tension $\mathbb{E}_1$ increases the size of the trapping bolus increases gradually. It can be examined from Fig. 7 that with the increment of mass characterization parameter $\mathbb{E}_2$ the number of the bolus remains constant whereas the magnitude of the bolus decreases gradually. It can be seen from Fig. 8 that with the rise of damping nature $\mathbb{E}_3$ the size of the trapping bolus decreases. It can be illustrated from Fig. 9 that when wall rigidity $\mathbb{E}_4$ increases the magnitude of the trapping bolus decreases. Fig. 10 is prepared for various values of

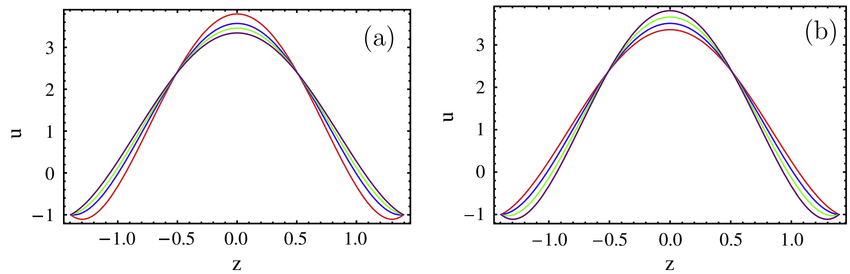

Figure 2 Velocity profile for fixed $\phi = 0.5, t = 0.05, \beta = 0.9, n = 1.5, \mathbb{E}_3 = 0.01, \mathbb{E}_4 = 0.2, \mathbb{E}_5 = 0.1, We = 0.01$. (a) red line: $\mathbb{E}_1 = 0.35$, blue line: $\mathbb{E}_1 = 0.40$, green line: $\mathbb{E}_1 = 0.5$, purple line: $\mathbb{E}_1 = 0.55$. (b) red line: $\mathbb{E}_2 = 0.1$, blue line: $\mathbb{E}_2 = 0.4$, green line: $\mathbb{E}_2 = 0.7$, purple line: $\mathbb{E}_2 = 1$.

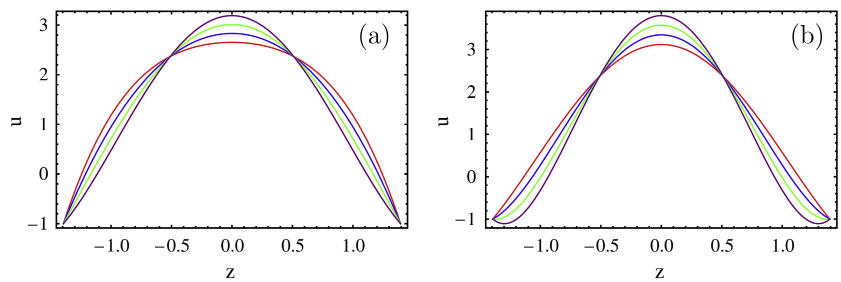

Figure 3 Velocity profile for fixed $\phi = 0.5, t = 0.05, \beta = 0.9, n = 1.5, \mathbb{E}_1 = 0.5, \mathbb{E}_2 = 0.3, \mathbb{E}_5 = 0.1, We = 0.01$. (a) red line: $\mathbb{E}_3 = 0.001$, blue line: $\mathbb{E}_3 = 0.003$, green line: $\mathbb{E}_3 = 0.005$, purple line: $\mathbb{E}_3 = 0.007$. (b) red line: $\mathbb{E}_4 = 0.05$, blue line: $\mathbb{E}_4 = 0.15$, green line: $\mathbb{E}_4 = 0.25$, purple line: $\mathbb{E}_4 = 0.35$.

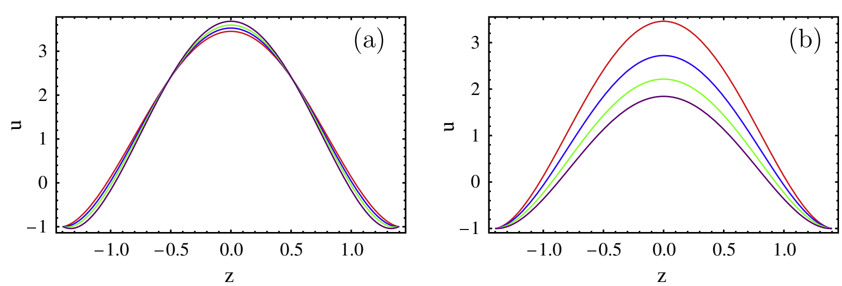

Figure 4 Velocity profile for fixed $\phi = 0.5, t = 0.05, \beta = 0.9, \mathbb{E}_1 = 0.5, \mathbb{E}_3 = 0.01, \mathbb{E}_4 = 0.2, \mathbb{E}_2 = 0.3, We = 0.01$. (a) red line: $\mathbb{E}_5 = 0.01$, blue line: $\mathbb{E}_5 = 1.3$, purple line: $\mathbb{E}_5 = 2.5$, green line: $\mathbb{E}_5 = 4$. (b) red line: $n = 1.5$, blue line: $n = 1.6$, green line: $n = 1.7$, purple line: $n = 1.8$.

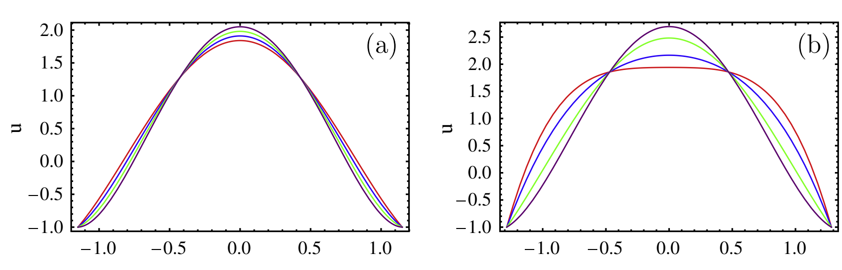

Figure 5 Velocity profile for fixed $\phi = 0.5, t = 0.05, \mathbb{E}_1 = 0.5, n = 1.5, \mathbb{E}_3 = 0.01, \mathbb{E}_4 = 0.2, \mathbb{E}_5 = 0.1, \mathbb{E}_2 = 0.3$. (a) red line: $We = 0.01$, blue line: $We = 0.02$, green line: $We = 0.03$, purple line: $We = 0.04$. (b) red line: $\beta = 0.3$, blue line: $\beta = 0.35$, green line: $\beta = 0.5$, purple line: $\beta = 9$.

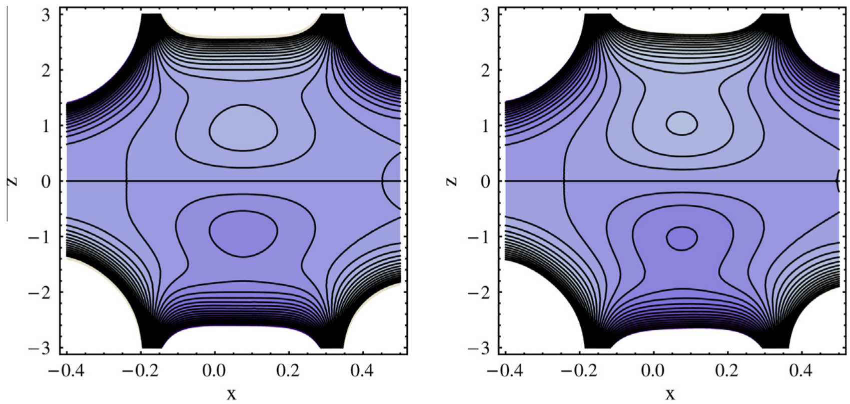

(a) $\mathbb{E}_1 = 0.25$ (b) $\mathbb{E}_1 = 0.40$

Figure 6 Stream lines for fixed $\phi = 0.5, t = 0.05, \beta = 0.9, n = 1.5, \mathbb{E}_3 = 0.01, \mathbb{E}_4 = 0.2, \mathbb{E}_5 = 0.1, \mathbb{E}_2 = 0.3, We = 0.01$.

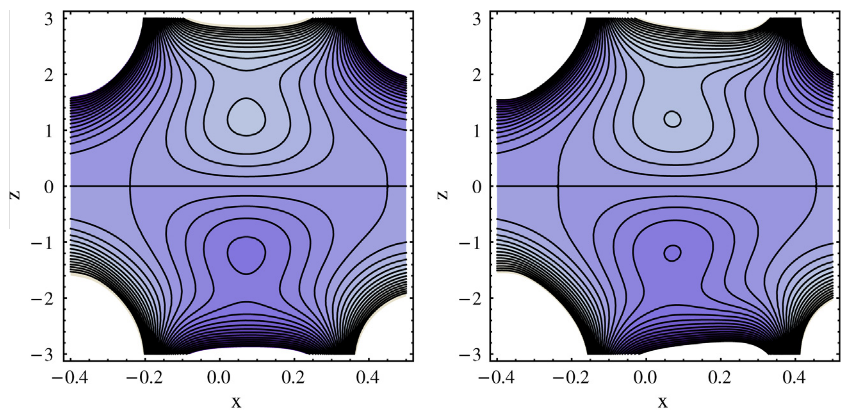

(a) $\mathbb{E}_2 = 0.1$ (b) $\mathbb{E}_2 = 0.40$

Figure 7 Stream lines for fixed $\phi = 0.5, t = 0.05, \beta = 0.9, n = 1.5, \mathbb{E}_3 = 0.01, \mathbb{E}_4 = 0.2, \mathbb{E}_5 = 0.1, \mathbb{E}_1 = 0.3, We = 0.01$.

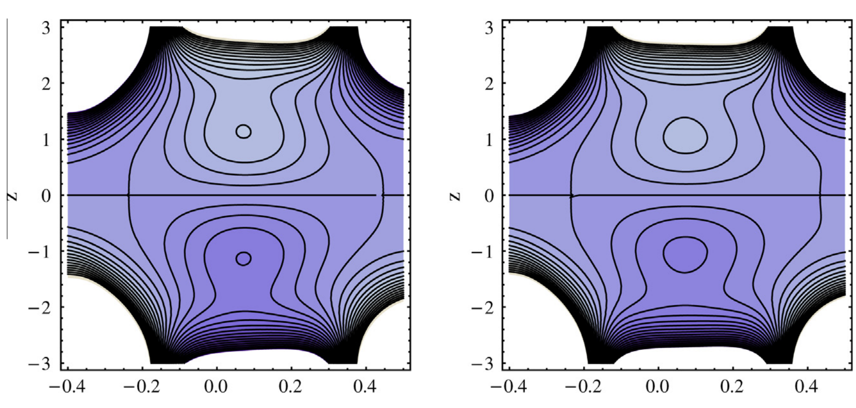

(a) $\mathbb{E}_3 = 0.006$ (b) $\mathbb{E}_3 = 0.008$

Figure 8 Stream lines for fixed $\phi = 0.5, t = 0.05, \beta = 0.9, n = 1.5, \mathbb{E}_2 = 0.3, \mathbb{E}_4 = 0.2, \mathbb{E}_5 = 0.1, \mathbb{E}_1 = 0.3, We = 0.01$.

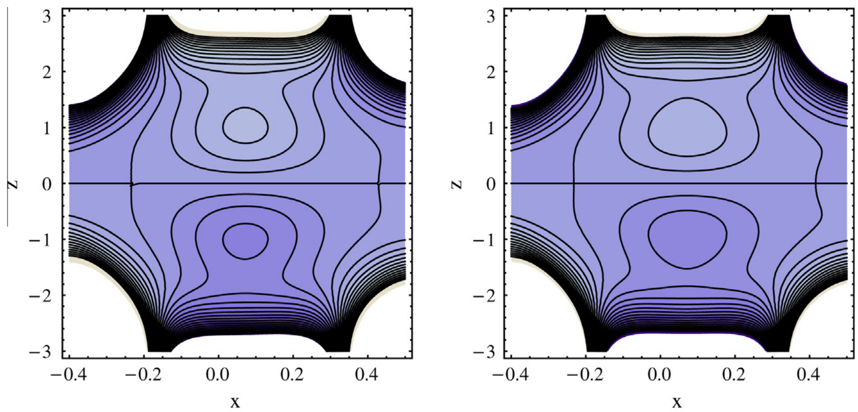

(a) $\mathbb{E}_4 = 0.15$ (b) $\mathbb{E}_4 = 0.25$

Figure 9 Stream lines for fixed $\phi = 0.5, t = 0.05, \beta = 0.9, n = 1.5, \mathbb{E}_2 = 0.3, \mathbb{E}_3 = 0.01, \mathbb{E}_5 = 0.1, \mathbb{E}_1 = 0.3, We = 0.01$.

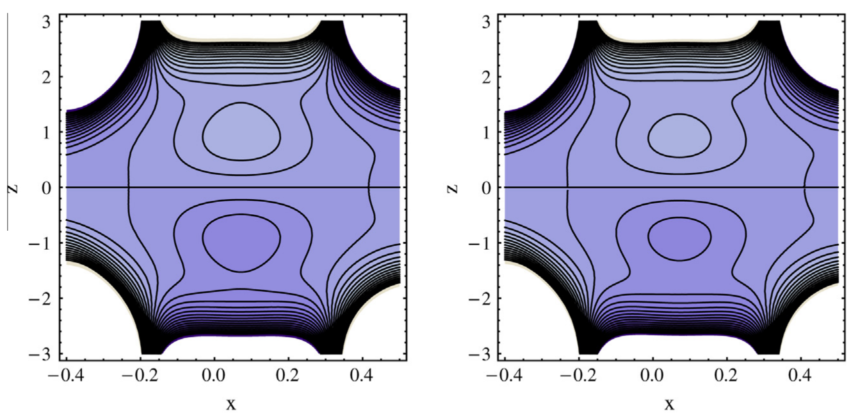

(a) $\mathbb{E}5 = 0\ .15$ (b) $\mathbb{E}5 = 0\ .25$

Figure 10 Stream lines for fixed $\phi = 0.5, t = 0.05, \beta = 0.9, n = 1.5, \mathbb{E}_2 = 0.3, \mathbb{E}_3 = 0.01, \mathbb{E}_4 = 0.2, \mathbb{E}_1 = 0.3, We = 0.01$.

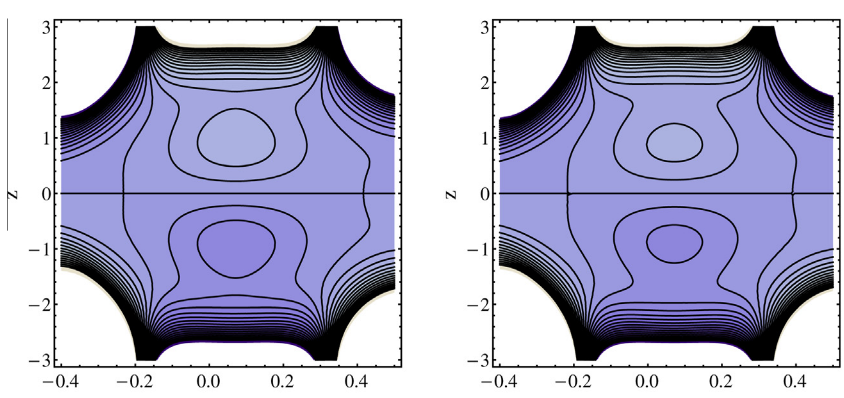

(a) $n = 1.5$ (b) $n = 1.6$

Figure 11 Stream lines for fixed $\phi = 0.5, t = 0.05, \beta = 0.9, \mathbb{E}_5 = 0.1, \mathbb{E}_2 = 0.3, \mathbb{E}_3 = 0.01, \mathbb{E}_4 = 0.2, \mathbb{E}_1 = 0.3, We = 0.01$.

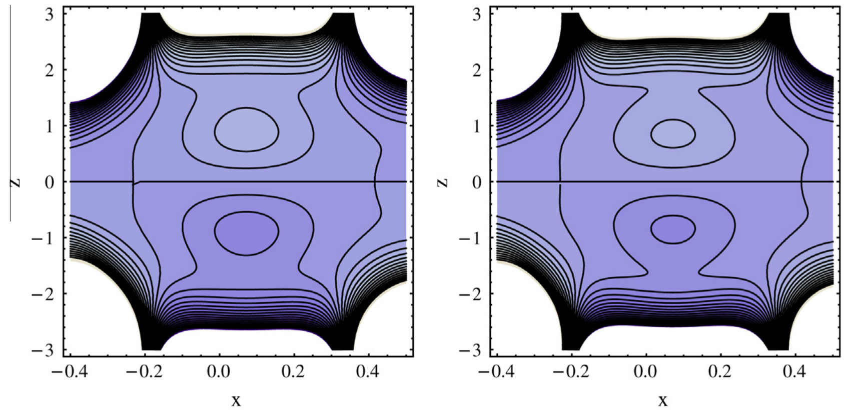

(a) $We = 0.02$ (b) $We = 0.04$

Figure 12 Stream lines for fixed $\phi = 0.5, t = 0.05, \beta = 0.9, n = 1.5, \mathbb{E}_2 = 0.3, \mathbb{E}_3 = 0.01, \mathbb{E}_4 = 0.2, \mathbb{E}_1 = 0.3, \mathbb{E}_5 = 0.1$.

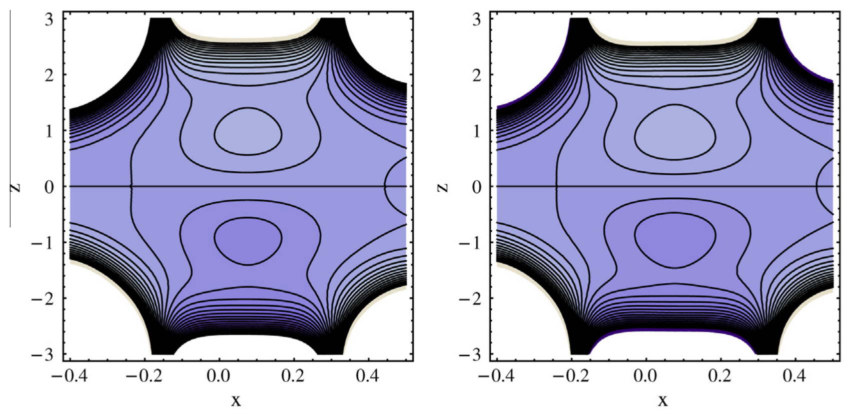

(a) $\beta = 0.6$ (b) $\beta = 1.5$

Figure 13 Stream lines for fixed $\phi = 0.5, t = 0.05, \mathbb{E}_5 = 0.1, n = 1.5, \mathbb{E}_2 = 0.3, \mathbb{E}_3 = 0.01, \mathbb{E}_4 = 0.2, \mathbb{E}_1 = 0.3, We = 0.01$.

Table 1 Comparison of velocity profile for Newtonian and non-Newtonian fluid for values of n [44].

$\mathbb{H}$	$u(y,z)$ $n = 0$	$u(y,z)$ $n = 1.5$	$u(y,z)$ $n = 1.6$	$u(y,z)$ $n = 1.8$
1.29	−1	−1	−1	−1
1.13	−1.6899	−0.6944	−0.7579	−0.8701
0.97	−2.1163	−0.1475	−0.3071	−0.5477
0.80	−2.3454	0.5260	0.2559	−0.1158
0.64	−2.4387	1.2248	0.8444	0.3503
0.48	−2.4504	1.8621	1.3838	0.7853
0.32	−2.4251	2.3684	1.8137	1.1358
0.16	−2.3963	2.6929	2.0898	1.3622
0	−2.3844	2.8045	2.1849	1.4404
−0.16	−2.3963	2.6929	2.0898	1.3622
−0.32	−2.4251	2.3684	1.8137	1.1358
−0.48	−2.4504	1.8621	1.3838	0.7853
−0.64	−2.4387	1.2248	0.8444	0.3503
−0.80	−2.3454	0.5260	0.2559	−0.1158
−0.97	−2.1163	−0.1475	−0.3071	−0.5477
−1.13	−1.6899	−0.6944	−0.7579	−0.8701
−1.29	−1	−1	−1	−1

wall elastance $\mathbb{E}_5$. We can observe from this figure that when wall elastance $\mathbb{E}_5$ increases the size of the bolus decreases gradually and the number of trapping bolus remains constant. It can be determined from Fig. 11 that when n increases then the size of bolus decreases slowly. In Fig. 12 we can see that with the increment of Weissenberg number We the size of the bolus increases. In Fig. 13 we analyze that when we increase than the size of the bolus increases. Comparison of velocity between Newtonian and non-Newtonian fluid is given in Table 1.

5. Conclusion

In this article, three dimensional peristaltic flow of hyperbolic tangent fluid with flexible walls has been investigated. The influence of wall properties has been discussed under the consideration of long wavelength and low Reynolds number. The governing equations of motion are modeled and solved with the help of homotopy perturbation method. The trapping phenomena of various physical parameters are sketched and discussed. The main findings of the present analysis are summarized below:

- Velocity field decreases with the increases of $\mathbb{E}_1, \mathbb{E}_2, \mathbb{E}_3$ near the walls but its opposite behavior has been observed in the middle of the duct.

- Velocity field decreases when fluid parameter n increases.
- Velocity field increases when $We, \mathbb{E}_4, \mathbb{E}_5$ increases in the center of the duct whereas its attitude is different close to the walls.
- When $\mathbb{E}_2$ and $\mathbb{E}_3$ increases the size of the trapping bolus decreases gradually.
- When $\mathbb{E}_4$ and $\mathbb{E}_5$ increases then the magnitude of the bolus decreases slowly whereas the number of the bolus remains constant.
- When β increases the velocity field increases.
- The size of the trapping bolus decreases gradually with the increment of fluid parameter n and We.

References

[1] T.W. Latham, Fluid motion in a peristaltic pump. M.Sc. thesis, MIT, Cambridge, 1966.
[2] A. Ebaid, Effects of magnetic field and wall slip conditions on the peristaltic transport of a Newtonian fluid in an asymmetric channel, Phys. Lett. A 372 (2008) 4493–4499.
[3] A.R. Rao, M. Mishra, Peristaltic transport of a power law fluid in a porous tube, J. Non-Newtonian Fluid. 121 (2004) 163–174.
[4] S. Das, R.N. Jana, Natural convective magneto-nano fluid flow and radiative heat transfer past a moving vertical plate, Alexandria Eng. J. 54 (1) (2015) 55–64.
[5] A.V. Mernone, J.N. Mazumdar, S.K. Lucas, A mathematical study of peristaltic transport of a casson fluid, Math. Comp. Model. 35 (2002) 895–912.
[6] D. Tripathi, Study of transient peristaltic heat flow through a finite porous channel, Math. Comp. Model. 57 (2013) 1270–1283.
[7] D. Tripathi, Peristaltic transport of a visco elastic fluid in a channel, Acta A stronaut. 68 (2011) 1379–1385.
[8] M. Kothandapani, S. Srinivas, On the influence of wall properties in the MHD peristaltic transport with heat transfer and porous medium, Phys. Lett. A 372 (2008) 4586–4591.
[9] S. Srinivas, M. Kothandapani, The influence of heat and mass transfer on MHD peristaltic flow through a porous space with compliant walls, Appl. Math. Comp. 21 (2009) 197–208.
[10] Y.A. Elmaboud, Kh.S. Mekheimer, Non-linear peristaltic transport of a second-order fluid through a porous medium, Appl. Math. Model. 35 (2011) 2695–2710.
[11] Y.A. Elmaboud, Kh.S. Mekheimer, A.I. Abdellateef, Thermal properties of couple-stress fluid flow in an asymmetric channel with peristalsis, J. Heat Transfer. 135 (4) (2013), http://dx.doi.org/10.1115/1.4023127.
[12] Y.A. Elmaboud, Influence of induced magnetic field on peristaltic flow in an annulus, Commun. Nonlinear Sci. Num. Simul. 17 (2012) 685–698.
[13] N.S. Akbar, Natural convective MHD peristaltic flow of a nanofluid with convective surface boundary conditions, J. Comput. Theor. Nanos. 12 (2) (2015) 257–262.
[14] N.S. Akbar, Heat transfer and carbon nano tubes analysis for the peristaltic flow in a diverging tube, Meccanica 50 (1) (2015) 39–47.
[15] N.S. Akbar, Application of Eyring-Powell fluid model in peristalsis with nano particles, J. Comput. Theor. Nanos. 12 (1) (2015) 94–100.
[16] N.S. Akbar, Natural convective MHD peristaltic flow of a nanofluid with convective surface boundary conditions, J. Comput. Theor. Nanos. 12 (2) (2015) 257–262.
[17] N.S. Akbar, Double-diffusive natural convective peristaltic flow of a Jeffrey nanofluid in a porous channel, Heat. Transf. Res. 45 (4) (2014).
[18] N.S. Akbar, Bioconvection peristaltic flow in an asymmetric channel filled by nanofluid containing gyrotactic microorganism: Bio nano engineering model, Int. J. Numer. Method. H 25 (2) (2015) 214–224.
[19] N.S. Akbar, Numerical and analytical simulation of peristaltic flow of a Jeffrey-six constant fluid, Appl. Anal. 94 (7) (2015) 1420–1438.
[20] N.S. Akbar, Entropy generation and energy conversion rate for the peristaltic flow in a tube with magnetic field, Energy 82 (2015) 23–30.
[21] G.C. Shit, M. Roy, Hydromagnetic effect on inclined peristaltic flow of a couple stress fluid, Alexandria Eng. J. 53 (4) (2014) 949–958.
[22] T.K. Mittra, S.N. Prasad, On the influence of wall properties and Poiseuille flow in peristalsis, J. Biomech. 6 (2012) 681–693.
[23] T.K. Mittra, S.N. Prasad, Interaction of peristaltic motion with poiseuille flow, Bull. Math. Biol. 36 (1974) 127–141.
[24] M.M. Rashidi, S.C. Rajvanshi, N. Kavyani, M. Keimanesh, I. Pop, B.S. Saini, Investigation of heat transfer in a porous annulus with pulsating pressure gradient by homotopy analysis method, Arab. J. Sci. Eng. 39 (2014) 5113–5128.
[25] K. Das, S. Jana, P.K. Kundu, Thermophoretic MHD slip flow over a permeable surface with variable fluid properties, Alexandria Eng. J. 54 (1) (2015) 35–44.
[26] R. Ellahi, M. Mubashir Bhatti, Ambreen A. Khan, Mathematical analysis of peristaltic transport of an eyring powell fluid through a porous rectangular duct, Wulfenia 22 (1) (2015) 266–283.
[27] R. Ellahi, M. Mubashir Bhatti, K. Vafai, Effects of heat and mass transfer on peristaltic flow in a non-uniform rectangular duct, Int. J. Heat Mass Transfer 71 (2014) 706–719.
[28] S. Akram, Kh.S. Mekheimer, S. Nadeem, Influence of lateral walls on peristaltic flow of a couple stress fluid in a non-uniform rectangular duct, Appl. Math. Inf. Sci. 8 (2014) 1127–1133.
[29] R. Ellahi, M. Mubashir Bhatti, A. Riaz, M. Sheikholeslami, Effects of magnetohydrodynamics on peristaltic flow of Jeffrey fluid in a rectangular duct through a porous medium, J. Porous Media 17 (2014) 143–157.
[30] M.V. Subba Reddy, M. Mishra, S. Sreenadh, A. Ramachandra Rao, Influence of lateral walls on peristaltic flow in a rectangular duct, ASME J. Fluids Eng. 127 (2005) 824–827.
[31] A. Riaz, R. Ellahi, S. Nadeem, Peristaltic transport of a Carreau fluid in a compliant rectangular duct, Alexandria Eng. J. 53 (2) (2014) 475–484.
[32] A.H. Shapiro, M.Y. Jaffrin, S.L. Weinberg, Peristaltic pumping with long wavelengths at low Reynold number, Fluid Mech. 37 (1969) 799–825.
[33] M.M. Rashidi, M. Keimanesh, S.C. Rajvanshi, Study of pulsatile flow in a porous annulus with the homotopy analysis method, Int. J. Num. Method Heat Fluid Flow 24 (2) (2011) 419–437.
[34] Kh.S. Mekheimer, Peristaltic flow of blood under effect of a magnetic field in a non-uniform channel, Appl. Math. Comp. 153 (2004) 763–777.
[35] M.A. Abd Elnaby, M.H. Haroun, A new model for study the effect of wall properties on peristaltic transport of a viscous fluid, Commun. Nonlinear. Sci. Num. Simul. 13 (2008) 752–762.
[36] N.S. Gad, Effects of hall currents on peristaltic transport with compliant walls, Appl. Math. Comp. 235 (2014) 546–554.
[37] Kh.S. Mekheimer, Y.A. Elmaboud, Peristaltic flow through a porous medium in an annulus: application of an endoscope, Appl. Math. Inf. Sci. 2 (2008) 103–121.
[38] G.C. Sankad, G. Radhakrishnamacharya, Effect of wall properties on peristaltic transport of micro polar fluid in a non-uniform channel, Int. J. Appl. Math. Mech. 6 (1) (2010) 94–107.

[39] A. Ebaid, Remarks on the homotopy perturbation method for the peristaltic flow of Jeffrey fluid with nano-particles in an asymmetric channel, Comp. Math. Appl. 68 (2014) 77–85.
[40] J.H. He, Application of homotopy perturbation method to nonlinear wave equation, Chaos. Solitons. Fract. 26 (2005) 695–700.
[41] J.H. He, Homotopy perturbation method for solving boundary value problems, Phys. Lett. A 350 (2006) 87–88.
[42] J.H. He, A note on the homotopy perturbation method, Therm. Sci. 14 (2010) 565–568.
[43] S. Nadeem, S. Akram, Peristaltic transport of a hyperbolic tangent fluid model in an asymmetric channel, Z. Naturforsch. A 64 (9–10) (2009) 559–567.
[44] S. Nadeem, A. Riaz, R. Ellahi, Peristaltic flow of viscous fluid in a rectangular duct with compliant walls, Comput. Math. Model. 25 (2014) 404–415.